Multichannel grazing-incidence spectrometer for plasma impurity diagnosis: SPRED

R. J. Fonck, A. T. Ramsey, and R. V. Yelle

A compact vacuum ultraviolet spectrometer system has been developed to provide time-resolved impurity spectra from tokamak plasmas. Two interchangeable aberration-corrected toroidal diffraction gratings with flat focal fields provide simultaneous coverage over the ranges 100–1100 Å or 160–1700 Å. The detector is an intensified self-scanning photodiode array. Spectral resolution is 2 Å with the higher dispersion grating. Minimum readout time for a full spectrum is 20 msec, but up to seven individual spectral lines can be measured with a 1-msec time resolution. The sensitivity of the system is comparable with that of a conventional grazing-incidence monochromator.

I. Introduction

The analysis of impurity behavior in high-temperature plasmas requires the observation of spectral lines from several stages of ionization for each major impurity species present.[1,2] Such observations are necessary in determining the ionic composition of the plasma, studying plasma–wall interactions, estimating power losses from impurity radiation, and providing a general monitor of discharge conditions. As tokamaks and other magnetically confined plasma facilities become more complex and less accessible, available observation time is becoming increasingly limited. Even with available observation time, plasma irreproducibility can cause large variations in line intensities. Thus experimental systems employing monochromators for monitoring impurity radiation are becoming obsolete, and the development of multichannel (both spatial and spectral) spectrometers has been receiving increased attention. In plasmas of thermonuclear interest, where central electron temperatures can reach several keV, the most intense emission lines of interest fall in the VUV spectral region. Since the signal from a standard grazing-incidence monochromator is often heavily polluted with scattered light, the ability to record both a line and its adjacent background radiation is an especially useful feature of the multichannel systems. Multichannel spectrometers scanning the 300–2000-Å region recently have been employed on several tokamaks[3–5] to provide broad spectral surveys. Spatially imaging systems using either rotating mirrors[6,7] or imaging detectors[8] have been used to provide monochromatic images of the radiation from tokamak impurities.

For routine monitoring of plasma impurity content there has been a need for a spectrometer that covers the 100–1100- or 100–1700-Å spectral range simultaneously with moderate spectral and temporal resolution. The 500–1600-Å range includes the major $\Delta n = 0$ transitions of common low-Z impurities (e.g., C and O) which radiate from the plasma periphery, while the 100–400-Å range contains important lines of highly ionized medium-Z impurities (e.g., Cl Ti, and Fe). These impurities are desorbed or sputtered from walls and limiters. The radiation from highly ionized atoms comes from the hot plasma core and can provide a sensitive local diagnostic of plasma properties.

This paper describes a multichannel spectrometer system which was developed to cover the 100–1700-Å range for use as a routine impurity monitor in tokamak plasmas. It also has sufficient flexibility to perform more specialized experiments such as following the behavior of artificially injected impurities with good time resolution. Design considerations included the desire for a compact physical package, a minimum number of moving parts, moderate spectral resolution (~2 Å), time resolution of the order of several milliseconds, high luminosity, good sensitivity down to at least 150 Å, and ultrahigh-vacuum compatability with synchrotron radiation sources for sensitivity calibration. To avoid a large investment in detector development the output format of the optical system was required to couple easily to an available multichannel detector. These requirements are all filled by the system de-

The authors are with Princeton University, Plasma Physics Laboratory, Princeton, New Jersey 08544.

Received 3 February 1982.

scribed here. It employs a toroidal holographically corrected diffraction grating which operates at a incident angle of 71° and gives a flat field spectrum. This spectrometer is referred to as the SPRED (survey, poor resolution, extended domain) spectrometer throughout this paper. This paper discusses the grating and optical system, the spectrometer and grating alignment procedure, and the detector. Finally, the performance of the entire SPRED system in laboratory tests and on the PDX tokamak is discussed, and representative data are presented.

II. Optical System

The heart of the spectrometer is a unique diffraction grating designed for the authors by the J-Y Optical Systems Division of Instruments SA, Inc. It is a Type IV diffraction grating in which the holographically recorded grooves are curved to place the desired spectral range on a flat focal field with optimal resolution. A schematic of the optical system is given in Fig. 1. The glass blank is a toroidal surface with a radius of curvature of 919 mm in the x-y (dispersion) plane of Fig. 1 and 102.5 mm in the y-z plane. The grooves were ion-etched into the glass substrate and overcoated with gold. The curvature of the grooves and the toroidal blank dimensions were adjusted to correct aberrations so that a flat focal field 40 mm wide was obtained. Two gratings have been made, one with a central groove density of 450 g/mm covering the 100–1100-Å spectral range over the 40-mm focal plane, the other with 290 g/mm covering 155–1700 Å. The ruled area on the grating blank is 22 mm wide (i.e., along the x axis) by 6 mm high (along the z axis). In typical operating conditions the grating is masked to a used area 21 mm wide by 3 mm high.

Detailed ray tracings were performed by ISA before fabrication of the gratings to fix design parameters, and some pertinent results of these calculations are noted here. The ray tracings assume an entrance slit 2 mm high by 25 μm wide, which are the usual operating values. The line shape over the focal plane of interest is symmetric, and the FWHM of the 450 (290)-g/mm grating is calculated to be 0.8 (1.25) Å. Astigmatism is zero for a point source on the optical axis of the entrance slit, while a point source at the top of the slit (1 mm off optical axis) is calculated to have a vertical extent of 0.13 mm at the exit plane. If exit slits of 2.5-mm height are used, there are no geometrical losses of light flux, resulting in a high luminosity. The gratings operate only in the condition shown in Fig. 1. The spectral range cannot be extended by rotating the grating because the aberrations for a new orientation of the grating are not sufficiently corrected to provide a high-quality spectrum across the flat field.

The location of the focal plane is given by

$$y = -26.6584\,x + 8162.12 \text{ mm} \tag{1}$$

in (x,y) coordinates with the grating centered at the origin. The wavelength is given as a function of distance along the focal plane by

$$k\lambda = d(\sin\alpha - \sin\beta), \tag{2}$$

$$l = \frac{b}{\cos\beta - m\sin\beta}, \tag{3}$$

$$S^2 = l^2 + l_1^2 - 2ll_1\cos(\beta - \beta_1), \tag{4}$$

where d^{-1} is the grating constant, l is the exit arm length from the grating center to the focal plane, and S is the distance along the focal plane from the lowest wavelength λ, with l_1,β_1 given in Fig. 1. From these relations it can be shown that the dispersion varies by <20% over the 40-mm long spectrum. To within 0.4 Å, the wavelength as a function of distance along the focal surface can be expressed by a cubic polynomial where the coefficients are found by fitting to a measured spectrum. The angle of incidence on the focal plane varies from 19 to 25°.

III. Mechanical System

A schematic of the entire SPRED system plus beam line coupling to a tokamak is shown in Fig. 2. The spectrometer housing plus grating mounts were designed and constructed by Schoeffel/McPherson Instruments to match the optical parameters of the gratings. The all-metal sealed chamber ensures a very clean ultrahigh-vacuum environment. The only component that does not have a metal seal is the detector assembly, where a high-vacuum epoxy is used to provide a metal-to-glass vacuum seal at the fiber-optic image conduit. (The detector assembly is described later.) A 20-liter/sec ion pump is sufficient to achieve a pressure of 5×10^{-8} Torr without baking. Isolation between the spectrometer vacuum and outside world is accomplished by use of a low-conductance entrance slit assembly connected via a bellows to a 1-mm wide by 5-mm high vacuum isolation slit located directly behind the entrance slit.

The two gratings are mounted on a rotary table and are interchangeable without breaking vacuum via a

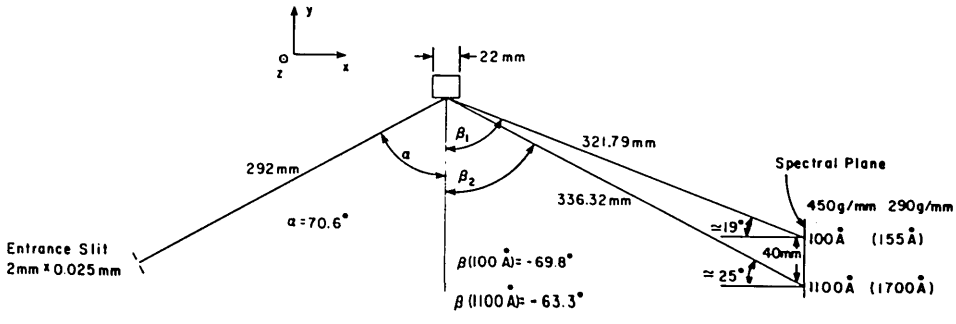

Fig. 1. Optical schematic and design specifications of the toroidal grating flat field spectrograph.

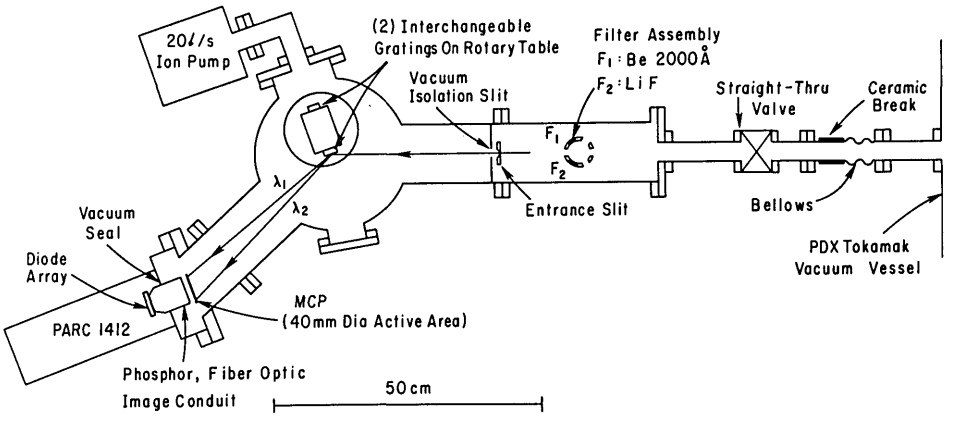

Fig. 2. Schematic of the SPRED system on the PDX tokamak.

rotary feedthrough. The grating positions are indexed by spring loading against a heavy pin, and the location of the spectrum is repeatable at the focal plane to within ±20 μm on grating exchange (or 0.4 Å with the 450-g/mm grating). Each grating mount provides adjustments for the six degrees of freedom needed to align the gratings. A focus adjustment (translation along the y axis in Fig. 1) is common to both gratings via a translating base and is adjustable without breaking vacuum. The gratings are masked by an adjustable aperture (not shown in Fig. 2) in front of the gratings on the entrance slit side of the optical path. As mentioned earlier, the grating mask was set to a used area 21 mm wide by 3 mm high.

Interchangeable fixed entrance slits are used, and the entrance slit assembly provides for a translation of the slit along the line connecting the slit and grating. An adjustable mask also allows variations of the effective entrance slit height. In all results reported here the entrance slit was 25 μm wide by 2 mm high in accordance with the conditions derived from the ray tracings for the gratings.

During fabrication of the spectrometer housing, scribe marks were made on the apparatus to allow mounting of thin wire cross hairs for defining the normal to the grating (the y axis), the optic axis through the entrance slit, and the zero-order beam exiting the spectrometer. Also the height of the optical plane was scribed around the inside of the vacuum chamber to facilitate alignment.

The filter assembly allows placement of a variety of filters in the beam line to provide separation between overlapping orders of diffraction. The ceramic break provides high-voltage electrical isolation from the tokamak, and the bellows is used for vibration isolation.

IV. Detector

The detector system used is a microchannel plate (MCP) image intensifier/converter which is fiber-optically coupled to a Reticon photodiode array (PDA). This detector is very similar to that originally described by Riegler and Moore.[9] A schematic of the detector head is shown in Fig. 3. A VUV photon is converted to a photoelectron and amplified by a microchannel plate.

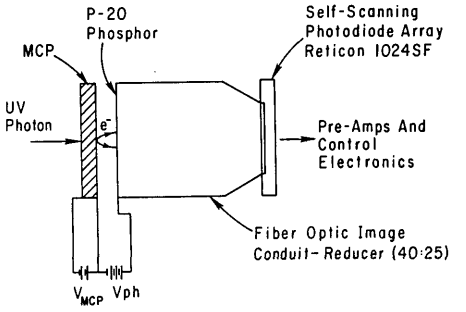

Fig. 3. Intensified photodiode array detector for 1-D VUV spatial imaging.

The exiting electrons are proximity focused and accelerated to impinge on a P-20 phosphor, which converts the electrons to visible light. The phosphor is coated on the input face of a fiber-optic image conduit/reducer which is in optical contact with the PDA. The high count rate capability, the large single-scan dynamic range, and the integrative nature of the intensified photodiode array make this a very useful detector for simultaneously observing both weak and intense tokamak emissions.

The MCP proximity focused image intensifier with the fiber-optic image conduit was supplied by Galileo Electro-Optics Corp. The MCP has a 40-mm diam active area and 12-μm pores with 15-μm center-to-center spacing. The front surface has a 1000-Å thick overcoating of Cu I to enhance its long wavelength sensitivity.[10] The MCP operating voltage is varied from 600 to 1000 V depending on applications. Over this range the electron gain varies from $\sim 4 \times 10^2$ to 3×10^4. In addition to converting the electron energy to visible radiation, the phosphor layer provides a gain of the order of 10–100 visible photons/incident 5-keV electron. This gain depends on the details of the phosphor layer but was found to vary like $V_{Ph}^{2.7}$ for one of the two intensifiers tested, and $V_{Ph}^{3.7}$ for the other.

The self-scanning photodiode array (Reticon 1024 SF) has 1024 pixels on 25-μm centers. Each pixel is 2.5 mm high, which is greater than the height required to intercept all rays from the 2-mm high entrance slit. The PDA is controlled and read out via an optical

multichannel analyzer (OMA) system from EG&G Princeton Applied Research Corp. The features and performance of this system without the image intensifier are described in detail by Talmi and Simpson,[11] and only some features are noted here. The OMA system allows a great deal of flexibility in controlling the readout of the PDA. The entire 1024 pixels can be read (full spectrographic mode) or selected portions thereof (partial spectrographic mode). Alternatively adjacent pixels can be grouped in a common datum readout and other pixels skipped to allow observation of specific spectral regions (polychromatic mode). To digitize and transmit the output from a given pixel in the spectrographic mode requires 16 μsec, while a pixel can be skipped in 0.5 μsec. Minimum scan time for the full spectrographic mode is 16 msec. For operation in the polychromator mode, up to seven separate spectral lines (i.e., pixel groups) can be sampled at a 1-kHz rate, while even more lines can be sampled at slower clock rates.

The OMA detector head (PARC 1412) and detector controller (PARC 1218) are used. The detector head is run evacuated to 200-μm Hg, and the PDA temperature is stabilized at -20°C with a thermoelectric cooler. The output from each pixel or group of pixels is digitized to 14-bit accuracy (16384 counts) with 1 count corresponding to ~1000 electrons. The PARC 1412 detector head was modified to include a fiber-optic faceplate on the Reticon chip, and the usual entrance window was removed to allow access for the image intensifier fiber-optic image conduit.

A block diagram of the detector electronics is shown in Fig. 4. The parallel data output from the PARC 1218 detector controller is interfaced directly to CAMAC dual-port memory modules (LeCroy 8801). These two memories each can hold 16K of 16-bit data. A CAMAC module developed at the Princeton Plasma Physics Laboratory (PPPL) provides the switching logic to synchronously fill these memory modules.[12] A data strobe for the memories is provided by the PARC 1218. The Nuclear Enterprises model 9017 16-bit output register supplies the required programming commands to the PARC 1218 to configure the PDA readout sequence. The clock provides a programmed series of trigger pulses, each of which initiates a scan of the PDA. For a typical spectrograph readout, 20-msec integration times may be used at discharge initiation and at the onset of neutral beam injection, while longer sample times (e.g., 40 or 100 msec) are used elsewhere during the quasi-steady state portion of the tokamak discharge. This feature minimizes the required memory space. The local CAMAC crate is fiber-optically coupled to the CAMAC highway to minimize noise pickup. A PDP-11, which is part of the general data acquisition system on the PDX tokamak, controls the CAMAC system.

V. Optical Alignment

Since this spectrograph system is of a novel design, it is worthwhile to describe the procedure followed for aligning the optical system. The mechanical alignment of the grating with respect to the entrance slit and detector relied on cross hairs placed across marks the

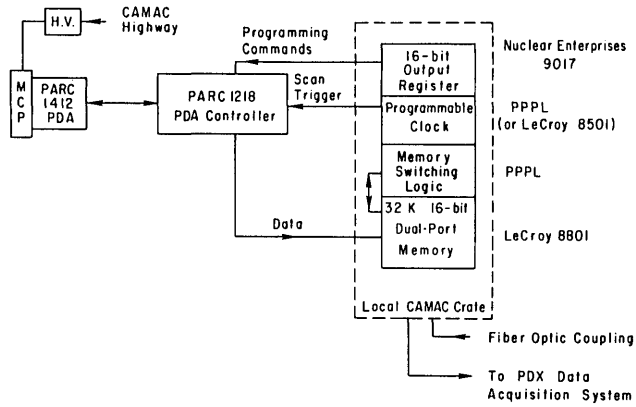

Fig. 4. Block diagram of electronics used to couple the photodiode array readout electronics to the local data acquisition system.

manufacturer had scribed on the vacuum housing. A He–Ne laser beam was directed along the desired normal to the grating through the front viewing port and back pump port (see Figs. 1 and 2). This defined the y axis in Fig. 1. In addition to the beam along the grating normal, a laser beam was directed through the center of the entrance slit and onto the grating. This beam had been centered in the entrance arm of the spectrometer, and the entrance slit had been mechanically centered in the arm and had been made vertical (i.e., parallel to the z axis) by aligning the single-slit diffraction pattern from the entrance slit along the optical plane. The grating was located in the x-z plane by adjusting its position until the center of the blank was coincident with the normal incidence beam. (The grating manufacturer specified that the optical center of the rulings is within ± 0.5 mm of the blank center.) Rotation about the z axis was set by returning the normal incidence beam on itself over a path length of ~2 m. Rotating about the y axis (i.e., making the grating rulings parallel to the entrance slit) was set by adjusting the diffracted beams from the normal incidence laser to lie on the optical plane. Because of the short radius of curvature of the toroidal blank in the vertical direction, rotation about the x axis could not be accurately set by autocollimation of the normal incidence beam, but was found to be best adjusted by vertically centering the beam incident through the slit on the zero-order cross hair at the exit port. That is, it was set to lie in the optical plane at the exit port. Finally the focus (i.e., displacement along the y axis) was mechanically set by having both laser beams intersect at the grating center and requiring the zero-order beam to exit on the zero-order cross hairs. Many of these adjustments interact, and a few iterations were necessary to achieve optimal alignment.

After the mechanical alignment for each of the two gratings was performed, a differentially pumped He hollow cathode discharge was used for further optical alignment. A spectrum was easily visible with the detector located at the position specified by the ray tracings. Care was taken to fill the optics with light so that false line profiles were not obtained. Spectral artifacts caused by ions or excited neutrals from the ion pump

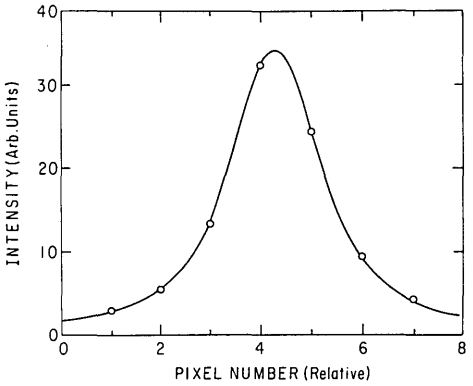

Fig. 5. Results of fitting the line profile at 304 Å to a convolution of a Lorentzian function with the photodiode array response function and the entrance slit. Open circles are the signals from individual pixels while the solid line is the fitted curve. FWHM of the fitted Lorentzian is 1.84 pixels.

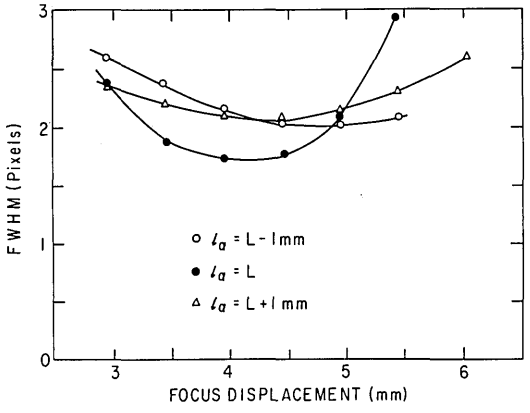

Fig. 6. Fitted FWHM (in pixels) of the 304-Å line as a function of focus position of the 450-g/mm grating. Curves are shown for three positions of the entrance slit. l_a is the distance from the entrance slit to the grating. L = 293.9 mm.

were removed by appropriate baffling of the pump and running at low spectrometer pressures.

The final optical alignment was achieved by minimizing the FWHM of the measured line profiles. The FWHM was determined by fitting the PDA output over a spectral line to a model line shape. An appropriate model was found to be a convolution of the pixel response function, a square function for the entrance slit, and a Lorentzian line shape. The Lorentzian arises from a convolution of the intrinsic line shape of the grating, the MCP line response function, and the charge spreading between the MCP and phosphor. As an example, Fig. 5 shows the result of a fit to the PDA response for the He II line at 304 Å. The FWHM is 1.8 pixels. With the 450-g/mm grating, this corresponds to a FWHM of 2.0 Å. (The image reduction ratio for this particular intensifier was 40:23.)

Only two degrees of freedom were adjusted during this optical alignment phase: the entrance arm length was varied, and the grating focus was optimized for each arm length. Varying the entrance arm length was the more sensitive adjustment for optimizing the alignment. Figure 6 shows a plot of the fitted FWHM as a function of displacement along the focus direction (i.e., the y axis) for three positions of the entrance slit. These data were sufficient to place the entrance slit at its optimal position. Also it was determined that the mechanical alignment of the grating had been accurate enough to place the grating focus to within 0.5 mm of its optimal position. Apart from rotating the PDA to the proper orientation with respect to the optical plane, no adjustments were necessary for the position of the detector system, which was held in a simple rigid mount. The relatively high f/No. of the optical systems ensures that the performance of the spectrometer is insensitive to defocusing effects.

As shown in Sec. VI, most of the remaining linewidth can be attributed to the charge spreading in the MCP phosphor interface, the MCP pore size, and the intrinsic spectrometer resolution. The above alignment procedure was sufficient to ensure that grating misalignment does not significantly contribute to the system resolution. The optimal focus positions of the two gratings were close enough to one another that the system does not have to be refocused on grating interchange.

VI. Performance

A. Resolution

The spatial resolution of the detector is primarily determined by charge spreading in the gap between the MCP and the phosphor. For a single straight-channel MCP which is run at a gain of 10^4 or less, space charge effects are not important,[13] and the charge spreading due to a point source of electrons in the channel is estimated by simple orbit theory to be

$$Y = 2\sin(2\theta)\frac{Us}{V_{\mathrm{Ph}}}\left(\sqrt{1+\frac{V_{\mathrm{Ph}}}{U\cos^2\theta}}-1\right), \qquad (5)$$

where Y is the diameter of the electron cloud at the phosphor surface, θ is the effective angle of the emitted electron relative to the channel axis (which is determined by the end spoiling depth), U is the mean electron energy at the end of the channel, V_{Ph} is the MCP–phosphor potential difference, and s is the separation between the MCP and phosphor surface.

Using the He hollow cathode source, measurements of the FWHM for 584 and 304 Å were made for various values of s and V_{Ph}. Two different intensifier–detector combinations were measured with two values of s for each intensifier assembly. The results of these measurements are shown in Fig. 7. The data points labeled Proto-SPRED were obtained with a prototype multichannel spectrometer,[4] which employed a Seyalike spectrometer whose resolution at the detector surface was comparable with that of the FWHM predicted from the SPRED grating ray tracings. The solid line in Fig. 7 is a fit of the data to the expression in Eq. (5) plus a constant offset. The fitted values were $\theta = 10.5°$, U = 30 V, and the constant = 50 μm. These values of θ and U are reasonable for a typical MCP.[14] The residual width of 50 μm compares favorably to the resolution expected from summing the MCP pore diameter, which

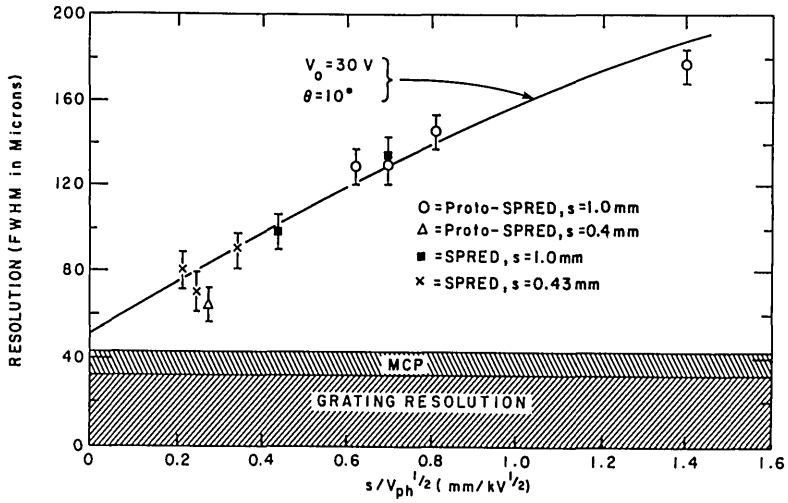

Fig. 7. SPRED resolution at focal plane as a function of intensifier parameters. Solid line is from Eq. (5), with U = 30 V and θ = 10.5° plus an offset of 50 μm. Grating resolution is the FWHM from the ray tracings for the 450-g/mm grating.

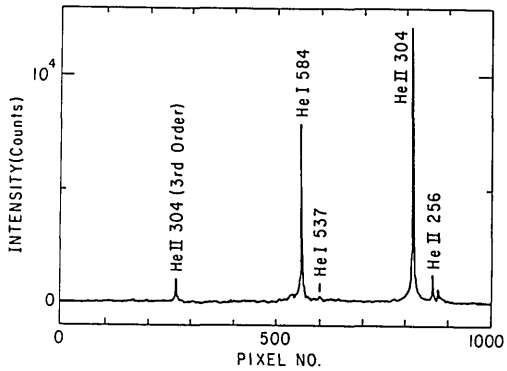

Fig. 8. Spectrum from a He hollow cathode discharge (450-g/mm grating; 50-μm entrance slit).

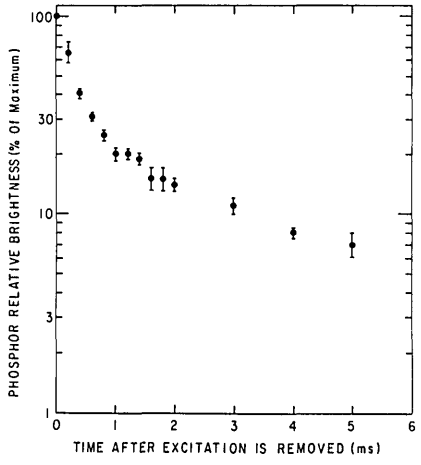

Fig. 9. Decay characteristic of intensifier phosphor output when the steady source is chopped off at t = 0. Intensifier MCP was excited with 2537-Å radiation.

is the FWHM of the MCP line response function,[15] and the calculated FWHM of the gratings for a 25-μm entrance slit width. A full He spectrum is shown in Fig. 8 for the higher dispersion grating. Fits to the stronger lines revealed no variation in resolution across the detector, verifying that the focus is indeed a flat field. From this it is concluded that the grating behavior agrees with that predicted by the ray tracings and that residual linewidth due to misalignment of the optics is minimal.

Since increasing the electric field in the MCP–phosphor interface eventually leads to breakdown, the choice of operating parameters requires a balance between desired resolution, which is determined by $s/V_{Ph}^{1/2}$ all else being equal, and gain, which scales as $V_{Ph}^{(3\text{ to }4)}$ (depending on the intensifier) for the intensifiers tested. With a clean vacuum, but without baking, V_{Ph} = 5 kV was obtained without breakdown with s = 0.43 mm. The chosen operating conditions were s = 0.43 mm and V_{Ph} = 4 kV.

B. Time Response

The readout electronics of the OMA system have a practical limit of ~1-msec sampling time. However, the fundamental limit of the time response of the detector to a transient light source is due to the decay time of the phosphoresence from the phosphor layer. The decay of the phosphor for one of the intensifiers used in these studies was measured by exciting the MCP with Hg I 2537-Å radiation chopped to a 80-Hz square wave. The phosphor output was measured both with an RCA 1P28 photomultiplier and with the PDA run with a 1-msec sampling time in the grouped pixel mode. The typical decay of the signal after the source is chopped off is shown Fig. 9. The decay is not exponential. The signal takes 0.5 msec to fall by a factor of $1/e$, while it takes 2.5 msec to fall to 10% and ~6 msec to fall to 5% of the original level. The MCP is always run so that the current density is <10% of the saturation current density, which in this case was ~2 μA/cm^2. The observed decay of the phosphor signal is consistent with the decay times expected for P-20 phosphor excited with a current density of 0.2 μA/cm^2.[16] Hence with this detector system there is no need to reduce the PDA integration time below 1 msec.

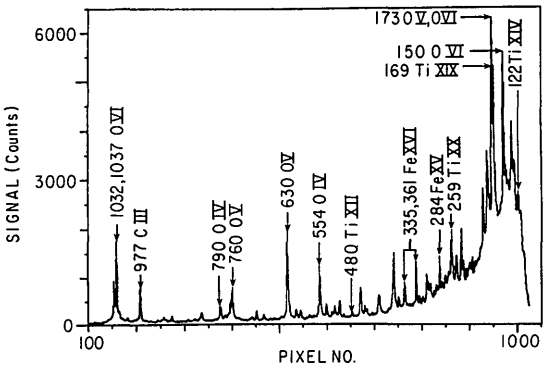

Fig. 10. Full SPRED spectrum using the 450-g/mm grating obtained from a ohmically heated circular discharge in the PDX tokamak.

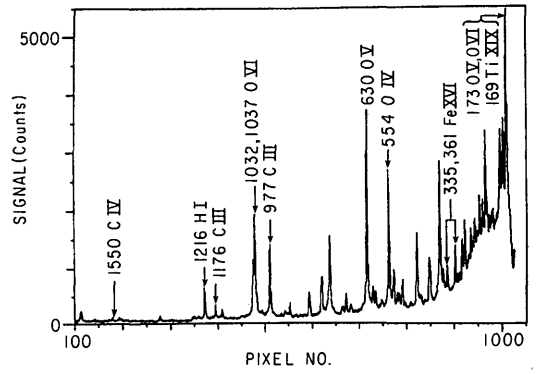

Fig. 11. Spectrum from PDX obtained with the 290-g/mm grating.

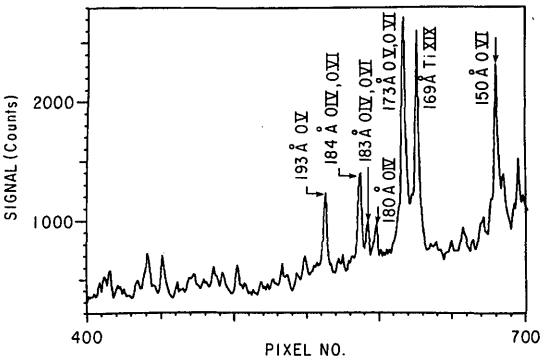

Fig. 12. SPRED spectra with a Be filter to suppress radiation above 400 Å. The third-order spectrum of the strong low wavelength emissions is resolved (450-g/mm grating).

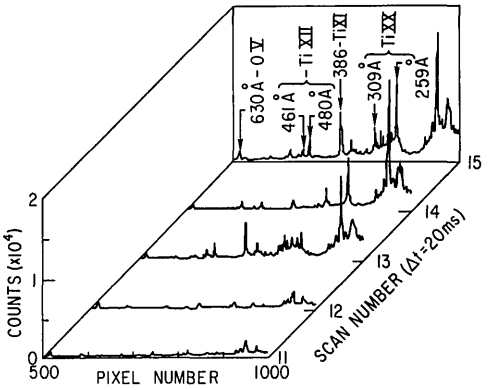

Fig. 13. Time evolution of low-wavelength PDX spectra bursting of titanium radiation.

C. Time-Resolved Tokamak Spectra

Figure 10 presents a spectrum obtained from an ohmically heated PDX discharge. At least thirty-two of these spectra are recorded each shot. The integration time was 20 msec. The reciprocal dispersion of the PDA is 1.1 Å/pixel. Strong emission lines are observed down to 130 Å, and lines from both low-Z edge impurities and highly ionized centrally localized metallic ions are all evident in this single readout. The broad feature at the lowest wavelengths is probably due to both blending of many unresolved lines and scattered light. A similar feature is seen in a spectrum obtained with the lower dispersion (290-g/mm) grating shown in Fig. 11. The brightest lines at low wavelengths are observed with higher resolution by observing them in third order. The relative intensities of lines in higher orders of diffraction are evident in Fig. 8. In particular, 304 Å has a value of >50:1 for the first- to second-order ratio while it is ~11:1 for first- to third-order. Figure 12 shows a spectrum taken with the 450-g/mm grating with a 2000-Å thick Be filter in the optical path to suppress wavelengths above ~400 Å. The 150–200-Å region is seen here clearly resolved.

A wavelength calibration for each grating was performed by fitting a cubic polynomial to express λ as a function of pixel numbers using measured positions of known lines. The fit had a standard deviation of ±0.2 Å across the field and systematic offsets of less than ±0.5 Å on repeated grating interchanges.

An example of the wealth of data which this system provides in a single shot is given in Fig. 13, which shows a partial time evolution of the low wavelength spectrum in a single PDX discharge. Only the short wavelength half of five of the thirty-two full spectral scans recorded are shown here. The sudden appearance of a group of lines at 200–300 Å and of the Ti XI and Ti XII lines in scan 13 are indicative of an influx of titanium into the discharge. Within 20 msec, by scan 14 these atoms have diffused into the hot plasma core and ionized up to produce strong Ti XIX and Ti XX lines. Before the atoms from the original event have left the plasma, another burst of Ti influx occurs in scan 15. Throughout these random bursts of Ti influx (whose origins are not well understood but are possibly due to arcing from the complex inner structure of PDX or to flaking of Ti layers deposited by Ti getter pumps) it is noted that oxygen radiation is unaffected. This information clearly would have required a very large number of reproducible discharges to have been obtained by a standard monochromator.

D. Polychromatic Operation

An example of the output of the SPRED spectrometer when operated in the polychromator mode is shown in Fig. 14. For this case, eight groups of pixels, ranging

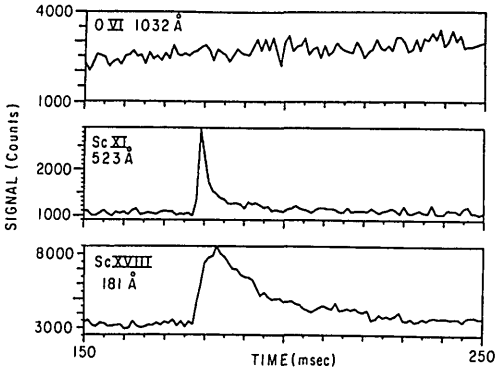

Fig. 14. Polychromatic output of SPRED showing time evolution of Sc spectral lines arising from laser blowoff injection of Sc into the PDX plasma. Integration time is 2 msec. This is raw data; background levels have not been subtracted.

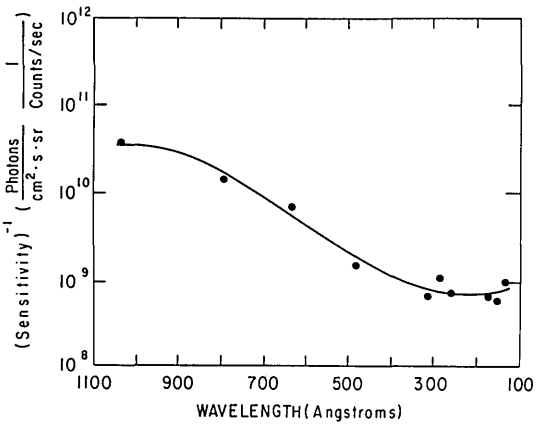

Fig. 15. Reciprocal sensitivity of the SPRED system as a function of wavelength for V_{Ph} = 4000 V, V_{MCP} = 800 V, 450-g/mm grating. Entrance slit was 2 mm × 25 μm, and grating area was 3 × 21 mm.

in sizes from 4 to 8 pixels and each covering a spectral line of interest, were sampled with a 2-msec integration time. The output of three of those groups is displayed in Fig. 14. The sudden rise in the ScXI 523-Å and Sc XVIII 181-Å lines is due to a short burst of Sc being injected into the discharge via laser ablation of a thin Sc film from a glass slide. As the Sc moves into the discharge it ionizes upward until it reaches a terminal stage of Sc XVIII or Sc XIX in the center of this discharge. The subsequent decay of Sc XVIII is due to the loss of Sc ions from the discharge. Throughout this injection process it is noted that the O VI 1032-Å radiation is unaffected by the Sc injection. Although it was not done for the data shown here, it is usually desirable to monitor the variation in background radiation in the spectrometer by recording pixel groups adjacent to those of interest.

E. Sensitivity

An estimate of the absolute intensity calibration for the SPRED system was obtained by comparing the response of the SPRED spectrometer with that of a grazing-incidence monochromator for a number of emission lines spanning the full spectral range. The grazing-incidence monochromator was absolutely calibrated via the branching ratio technique[17] and viewed the plasma 120° toroidally around the tokamak from the SPRED spectrometer. Toroidal asymmetries may decrease the accuracy of this sensitivity calibration transfer. The results of the absolute calibration of SPRED are shown in Fig. 15 for the 450-g/mm grating. The solid line is a polynomial fit to the data points. At best this initial calibration is good to ±50%. The larger sensitivity at low wavelengths is presumably because the grating is a laminar grating which results in a blazed efficiency peak near zero order.

F. Noise Level and Dynamic Range

The dynamic range is determined by the maximum signal obtainable and the noise level. At best the noise due to the PDA system is dominant. The major sources of noise in the photodiode output are dark current shot noise and readout noise. A photodiode array has fixed

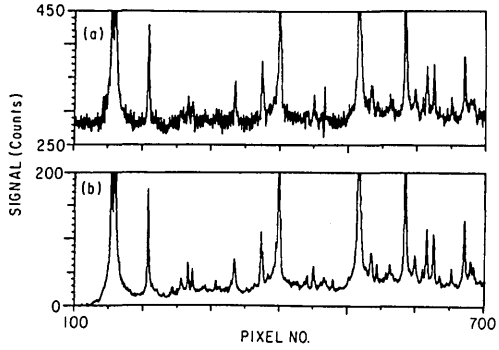

Fig. 16. Example of fixed background compensation: (a) raw data from PDX plasma; (b) data in (a) with a dark scan subtracted to remove the fixed pattern background.

pattern noise due to transient signals being coupled to the video lines by external stray capacitances and a noise level that occurs due to uncertainty in resetting each diode during the readout process. Also, preamplifier noise can contribute to the overall noise level.[11] Since the PDA is cooled to −20°C, dark current noise is negligible for the short integration times used here. The fixed pattern background noise is eliminated by recording a dark scan periodically and subtracting it from a data scan. The results of such a background subtraction is shown in Fig. 16. The 300 counts of fixed background noise are eliminated, and weak spectral features are revealed where they are not evident in the raw data scan. The residual readout noise level was measured to have a rms value of <1 count in a controlled laboratory setting but increased to ~2 counts rms in the electrically hostile tokamak environment. The output of a pixel of the PDA saturates at 16,384 counts (14 bits) and is linear up to that level.[11] A measurement of the intensity ratio of a strong spectral line to a weak line showed no variation (within ±5%) as a function of V_{Ph} and V_{MCP}. The stronger line was driven almost to saturation of the ADC for the PDA output. This indicates that the MCP/intensifier output was not saturating, and that the signal gain can be considered linear

over the full output range of the PDA. Thus the dynamic range in a single spectral scan is $\sim 10^4$:1, which is very useful since tokamak spectra have both very strong and very weak spectral features of interest in a single discharge.

In addition to the large dynamic range in a single scan, the effective range of sensitivity of the system can be varied by a factor of 100 by adjusting the MCP operating voltage over the 650–1000-V range and V_{Ph} from 4 to 5 kV. Without an extremely clean vacuum the noise level does increase somewhat when V_{Ph} is increased from 4 to 5 kV; presumably this is due to microarcing between the MCP and phosphor.

Finally, from Fig. 16 it is seen that one can easily measure a spectral line that is, say, 20 counts high. At 300 Å the sensitivity of SPRED is $\sim 9 \times 10^{11}$ photon/cm^2 sec sr/count/msec. Assuming a 20-msec integration time, this implies that an isolated line whose intensity is 1×10^{12} photon/cm^2 sec sr is readily measurable in the spectrographic mode, which compares favorably with the sensitivity and SNR of a conventional grazing-incidence monochromator at that wavelength.

VII. Conclusion

The SPRED spectrometer system is a novel multichannel spectrometer that provides simultaneous observation of the 100–1100-Å (or 155–1700-Å) spectral range with moderate resolution. The sensitivity is usable down to ~125 Å, with peak sensitivity in the 150–300-Å range, and is comparable with typical grazing-indicence monochromators used on tokamak facilities. The spectral resolution of 2 Å is acceptable for many spectroscopic studies of tokamak plasmas. The system offers a compact, rugged physical package with a minimum of moving parts. The optical system performs as well as expected from the ray tracings and design specifications. The present system resolution is limited by the grating resolution and the proximity-focused intensifier in the detector. It is possible that future improvements in detector technology will allow one to use this spectrometer at a resolution limited solely by the optical system. The wide range of choices in modes of operation as provided by the OMA readout electronics allow trade offs to be made consistent with the experiment of interest. This flexibility in choosing among time resolution, spectral resolution, time range, and spectral range keeps the required local CAMAC memory and final disk storage space to a minimum.

The utility of the SPRED system as a qualitative impurity monitor for high-temperature plasmas is evident. It allows simultaneous observation of most major impurity species in a tokamak plasma. With absolute intensity calibration and a shot-to-shot spatial scanning capability, the system can reduce the plasma shots required to produce impurity spatial distributions for several ion stages of several impurity species by a factor of 10 to 20. This is an important gain in capability as magnetically confined plasma facilities become increasingly more complex and less accessible. The use of a fast scanning mirror operating at grazing incidence to sweep the spectrometer field of view across the plasma could result in obtaining spectral and spatial resolution in a single discharge. Even without further development and without a spatial scanning capability, spectra from the SPRED system described here, coupled with simple impurity transport models, can provide estimates of impurity concentrations and radiated power with data from a single tokamak discharge.[18]

The authors acknowledge encouragement from D. Meade and E. Hinnov during the development of this project. Useful discussions with R. Bell and W. Moos of The Johns Hopkins University are also appreciated. J. Lerner of ISA provided much help and guidance in the development of the specifications for the toroidal gratings and in the understanding of these gratings thereafter. R. Deneault and his co-workers at Schoeffel/McPherson were responsible for the design and fabrication of the spectrometer housing with the grating holder and entrance slit assemblies. V. Braco and P. Roney developed most of the software needed to collect and display data on the PPPL data acquisition system. Finally, members of the PDX operating crew are thanked for their cooperation and for providing the observed plasma discharges.

This work was supported by DOE contract DE-AC02-76-CHO-3073.

References

1. R. C. Isler, E. C. Crume, and H. C. Howe, Nucl. Fusion **19,** 727 (1979).
2. R. J. Hawryluk, S. Suckewer, and S. P. Hirschman, Nucl. Fusion **19,** 607 (1979).
3. R. J. Groebner and R. N. Dexter, Plasma Phys. **23,** 693 (1980).
4. A. T. Ramsey, R. J. Fonck, and R. V. Yelle, Bull. Am. Phys. Soc. **25,** 938 (1980).
5. R. E. Bell, M. Finkenthal, and H. W. Moos, Rev. Sci. Instrum. **52,** 1806 (1981).
6. C. Breton, C. DeMichelis, M. Finkenthal, and M. J. Mattioli, J. Phys. E **12,** 894 (1979).
7. S. Suckewer, H. P. Eubank, R. J. Goldston, E. Hinnov, and N. R. Sauthoff, Phys. Rev. Lett. **43,** 207 (1979).
8. R. K. Richards, H. W. Moos, and S. L. Allen, Rev. Sci. Instrum. **51,** 1 (1980).
9. G. R. Riegler and K. A. Moore, IEEE Trans. Nucl. Sci. **NS-20,** 102 (1973).
10. R. K. Richards, Rev. Sci. Instrum. **49,** 1210 (1978).
11. Y. Talmi and R. W. Simpson, Appl. Opt. **19,** 1401 (1980).
12. R. V. Yelle, R. J. Fonck, H. Ogawa, and F. Senk, to be submitted for publication to Rev. Sci. Instrum.
13. R. Hutter, in *Focusing of Charged Particles*, A. Septier, Ed. (Academic, New York, 1967), Vol. 2.
14. J. G. Timothy and R. L. Bybee, Appl. Opt. **14,** 1632 (1975).
15. E. H. Eberhardt, ITT Electro-Optical Products Division Technical Note 127 (Aug. 1980).
16. *Optical Characteristics of Cathode Ray Tube Screens*, TEPAC Publication 116 (Electronic Industries Association, Washington, D.C., 1980).
17. E. Hinnov and F. W. Hofmann, J. Opt. Soc. Am. **53,** 1259 (1963).
18. R. J. Fonck, G. L. Schmidt, and T. McBride, Bull. Am. Phys. Soc. **26,** 864 (1981).